ESTIMATED EVOLUTION OF THE SPEED OF POWDER, WET AND TRANSITIONAL AVALANCHES BETWEEN TWO WIDELY SPACED LOCATIONS AT THE VDSL EXPERIMENTAL SITE EXTRACTED FROM THE ANALYSIS OF SEISMIC SIGNALS.

Emma Suriñach[1,4*], Elsa Leticia Flores-Márquez[2], Cristina Pérez-Guillén[1,3], Pere Roig-Lafón[1], Mar Tapia[4], Glòria Furdada[1]

[1]RISKNAT Avalanches Research Group- Institut Geomodels, Universitat de Barcelona (UB). Barcelona 28008, Spain
[2] Instituto de Geofisica, UNAM, Circuito Instituto S/N, Coyoacán, 04510 CDMX, México
[3] Graduate School of Environmental Studies, Nagoya University, Nagoya, Japan
[4]Laboratori d'Estudis Geofísics Eduard Fontserè (LEGEF-IEC), Barcelona 08001, Spain

ABSTRACT: The evolution of a snow avalanche descending along a path is reflected in the evolution of the frequency content of the generated seismic signals (spectrograms) recorded by seismic sensors located along the avalanche path. The wave transmission characteristics in the ground account for this. The analysis of spectrograms of seismic signals generated by snow avalanches of different size and type that descend along the same path at the Vallée de la Sion (VdLS, Valais, Switzerland) experimental site (SFL, Davos) allows us to estimate features related to the evolution of avalanche flow behavior. Given that the frequency content in the spectrograms increases in time as the avalanche approaches the sensor owing to the attenuation of seismic waves, the evolution of an avalanche can be estimated from the exponential function of time in the form $F(t) = K' e^{\beta t}$ fitted in the spectrograms. The avalanche speed is involved in β. The values of the coefficients of the fits obtained for the three different types of avalanches are included in three ranges. We treat the spectrograms as an image to apply the Hough Transform (HT) to obtain the parameters of its shape. For the highest location, in the avalanche track-zone, the curves collapse (are grouped) reflecting different tendencies according to the type of avalanche. The curves at the lowest location are gentler and show a more homogeneous behavior regardless of the type of avalanche. Nevertheless, the peculiarities of each type persist, although the fitted curves for the powder avalanches and transitional avalanches are more prone to collapse than those of wet avalanches. Our results show the feasibility of classifying the type of avalanche using the characteristics of the frequency-in-time evolution of avalanche seismic signals. Estimates of the mean speeds of the approaching avalanches were calculated at the recording sites.

KEYWORDS: avalanche dynamics, seismogram, spectrogram, Hough Transform, speed, evolution

1. INTRODUCTION

Snow avalanches are large moving masses that are sources of seismic energy that generate seismic wave fields (Suriñach et al., 2001). The wave field is mainly generated by the snow entrainment, friction, and impact on obstacles in the avalanche path. The movement of the ground caused by the passage of the seismic waves gives rise to the three component seismograms. Spectrograms are a 3D representation of the seismograms *S*(*t, f*) that indicates the evolution in time of the frequency content of the signal. Spectrograms corresponding to avalanches that approach a sensor display a shape that can be divided into the sections previously defined (Pérez-Guillén et al., (2016) and references therein): SON (Signal ONset), SOV (Signal Over) and SEN (Signal End) depending on whether the avalanche approaches the sensor, is over the sensor or is moving away from the sensor. The analysis of hundreds of seismograms of different snow avalanches indicates a close link between the quasi-exponential shape displayed by the SON sections of the spectrogram and the characteristics of the avalanche. Figure 1 shows the spectrograms of the seismic signals for the three types of avalanche investigated. Our study seeks to extract information from the spectrograms of the signals obtained at two widely spaced sites along the avalanche path in order to better understand the evolution of avalanches descending along this path. We considered the spectrograms as an image, and by applying image processing, we obtained parameters using the Hough Transform (HT). We applied the methodology to the data obtained at the Vallée de la Sion test site (Figure 2). This experimental site is

* *Corresponding author address:*
Emma Suriñach, Fac. Ciències de la Terra, Universitat de Barcelona (UB). C/Martí i Franquès s/n., Barcelona 08028, Spain;
tel: +34934021386;
email: emma.surinach@ub.edu

equipped with different instruments to monitor the avalanches that are released artificially or naturally (Sovilla et al., 2003 and references therein).

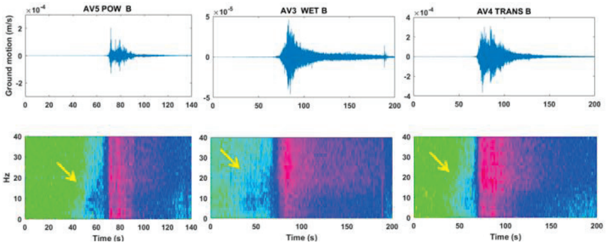

Figure 1: Spectrograms (colors in dB) of the seismic signals recorded at B for the three types of avalanche studied (left to right: powder, wet, transitional). The arrow indicates the SON section in each spectrogram.

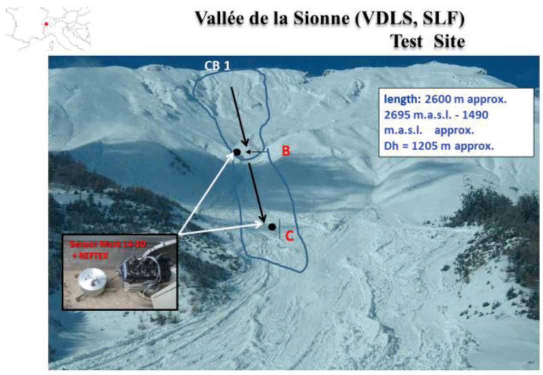

Figure 2: VdLS experimental site with the location of the recording sites B and C and the avalanche path (photo: SLF courtesy). Inset: seismic station

2. THEORY

2.1 Theoretical interpretation of the shape of the spectrogram

One interesting feature of the SON section of the spectrograms is the increase in amplitudes of the frequencies in time in a quasi- exponential shape. This feature results from the waves generated by the avalanche as it approaches the sensor because of the properties of the wave transmission in a medium, i.e. the effect of the attenuation (anelastic/intrinsic and geometrical spreading (e.g. Stein and Weisson, 2003) of the seismic waves in a medium, and the entrainment of snow as the avalanche descends along the path. In order to reproduce the shape of a spectrogram, we first obtain the equation of the amplitude decrease of a wave at a point as the distance increases from the source. Reversing the situation, we may assume that an amplitude increase will appear when the source approaches the point, the same equation being valid.

This is the case of the signals recorded in a given sensor as the avalanche approaches. Eq. (1) accounts for the decrease in the signal amplitudes *A(t',f)* at the sensor at distance *r(t')* from the source, where A_s *(t', f)* is the amplitude at the start of the avalanche and γ is the ratio of the increase in amplitude owing to the incorporation of snow as the avalanche approaches the sensor.

$$A(t',f) = \frac{A_s(t',f)}{k\sqrt{r(t')}}\; e^{-(\alpha(f)-\gamma)\, r(t')} \quad (1)$$

With $$\alpha(f) = \frac{\pi f}{Q(f)c(f)} \quad (2)$$

and $k = \sqrt{2\pi h}$ a constant. In eq. (1), surface waves were considered (Vilajosana et al., 2007). This equation considers the energy flux of the seismic wave through a cylindrical surface of radius *r(t')*, varying in time, and height *h*. *Q(f)* is the ground quality factor and *c(f)* the phase velocity of the surface waves. Eq. (1) can be simplified as

$$\mathrm{A}(t',f) = \mathrm{K}\,(t',f)\,\mathrm{e}^{-\beta'\, f)\, t'} \quad (3)$$

where we consider $r(t') = v_a(t')t'$, $v_a(t')$ being the speed of the avalanche, $\mathrm{K}(t',f) = \frac{A_s(t',\ f)}{k\sqrt{r(t')}}$

and $$\beta'(f,t') = (\alpha(f) - \gamma)\, v_a\,(t') \quad (4)$$

Eq. (3) is a decreasing function in time, the origin of which is the energy source. *r(t')* increases in time as the avalanche approaches the sensor. The amplitudes in our spectrograms increase in time. This is because the sensor is fixed and is the source that is moving towards it. Therefore, a change of the time/distance reference is necessary. In this case eq. (3) becomes

$$A(t,f) = \mathrm{K}\,(t,f)e^{\beta'(f,t)t} \quad (5)$$

Where *t* accounts for the change of reference (*t* = -*t'*). *β' (f, t)* depends on the avalanche speed $v_a(t)$ and on the frequency (as well as on *Q*(*f*) and *c*(*f*)).

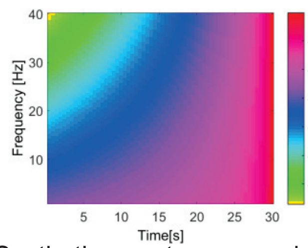

Figure 3: Synthetic spectrogram using eq. (5) for *As (t, f)* =1 m/s and *γ*= 0.002 m^{-1} (colors in dB).

Figure 3 shows a synthetic spectrogram using eq. (5) for *As (t, f)* =1 m/s and γ= 0.002 m^{-1}.

2.2 Hough Transform (HT) method

The Hough Transform (HT) (Hough,1962) was used to apply digital image processing to the spectrograms. The spectrogram amplitudes (Figure 4 a) were previously band-pass filtered (for all the times and the complete set of frequencies), selecting the band that was of interest to highlight. A process of binarization of the filtered image of the spectrogram enabled us to distinguish the arrival of the frequencies with most energy (Figure 4b). The image was convolved with an edge detector mask (Ridler and Calvard, 1978) to reinforce the lines of interest after changing the coordinates between the originals of the spectrogram (*t*, *f*) and those of the binary image (*x*, *y*). Finally, the HT was applied to the final binary image (black and white), where the straight lines are defined by the boundary between black and white, the black corresponding to the background. For each spectrogram, different fits defined by parameters A_i (slope) and B_i (*y*-intercept) were obtained through the application of the HT (Figure 4c). The slope (***a***) and the y-intercept (***b***) selected corresponded to the mean of all the possible fits. After a change of variable and of representation, the function obtained becomes

$$F(t) = \boldsymbol{c}\, e^{\boldsymbol{a}\, t} \qquad (6)$$

which represents the frequency as a function of the time of the spectrogram (Figure 4d).

A link between eq. (5) and eq. (6) is necessary, i.e. between a and c and the coefficients Κ and β'. First of all, an analysis of the dependence of the parameters in frequency is required. Note that the HT method uses a binarization process and, for each time, it discriminates the amplitudes to determine the shape of the SON section of the spectrogram using a threshold value. In Eq. (1), r (t') and *γ* are frequency independent. The effect of these variables is, in each time, an increase in all the amplitude values in the same ratio. As a result, the rate of the amplitude values for the threshold does not change when applying the HT. We may, therefore, assume that Κ is constant, termed Κ', for each spectrogram and then eq. (5) becomes

$$A(t, f) = \mathrm{K}' e^{\beta(f,t)t} \qquad (7)$$

where γ=0 ($\beta\,(f,t) = \alpha(f) v_a\,(t)$). Consequently, we can compare eq. (6) and eq. (7), assuming that the amplitudes of the spectrogram follow eq. (8), where β is considered constant.

$$\mathrm{F}\,(t) = \mathrm{K}'\, e^{\beta t} \qquad (8)$$

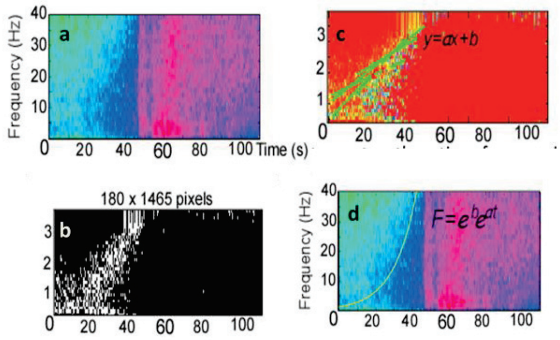

Figure 4: Images of the Hough Transform (HT) method (see text for explanation)

Avalanche Type (+)	Code (*)	K'_B (Hz)	β_B (s^{-1})	$\sigma_{\beta B}$ (s^{-1})	K'_C (Hz)	β_C (s^{-1})	$\sigma_{\beta C}$ (s^{-1})
Av1 POW-L	2003_504	0.04	0.19	0.68			
Av2 TRANS-L	2010_0003	0.29	0.11	0.48			
Av3 WET-M	2013_3018	2.67	0.07	0.11	6.02	0.05	0.13
Av4 TRANS- L	2013_3019	1.13	0.10	0.07	2.5	0.05	0.03
Av5 POW- M	2013_3024	0.09	0.14	0.12	0.23	0.09	0.18
Av6 WET-M	2013_3050	1.20	0.05	0.02	1	0.06	0.02
Av7 WET-M	2013_3053	3.84	0.06	0.09	1.5	0.03	0.01
Av8 POW-L	2015_17_2	0.70	0.31	0.10	1.2	0.09	0.07
Av9 POW-M	2011_3012	0.18	0.22	0.26	3.21	0.10	0.03
Av10 WET-S (PS)	2011_3023	6.40	0.05	0.05	11.1	0.08	0.08
Av11 TRANS-L	2013_3021	6.00	0.06	0.03	0.011	0.12	0.90
Av12 TRANS-L(WL)	2013_3020	0.20	0.11	0.08	7.1	0.07	0.09

Table 1: *K'*, *β*, and the standard deviations of *β* (σ_β) of the avalanches signals recorded at sites B and C. (+) Type after Pérez-Guillén et al., (2016). Previous classification in parenthesis. (*) SLF internal code.

3. DATA PROCESSING

We selected the seismic signals generated by twelve snow avalanches descending along the same path at the Vallée de la Sion (VdLS, Valais, Swiss) experimental site (SFL, Davos) and recorded at two sites (B and C) 690 m apart (Figure 1) along the path. Table 1 lists the avalanches identified as powder (POW), wet (WET), and transitional (TRANS) (Pérez-Guillén et al., 2016). The seismic data were obtained at stations consisting of a three-component seismometer Mark of 1Hz of eigenfrequency and a data acquisition system Reftek–130. Data, collected at 100 s.p.s., were transformed into ground velocity (m/s). All signals were band-pass filtered [1-40] Hz with a 4th- order Butterworth filter. The three seismic components of the ground motion (ms^{-1}) were merged into one Total Seismic Vector (TSV(t)) (ms^{-1}) following the criterion of vectors. Spectrograms were calculated for all the signals using the short-time FFT with a Hanning window (length 0.64s) and 50% (0.32s) of overlap. Figure 1 shows the TVS time series and spectrogram for each type of avalanche. We treated the SON section of the spectrograms of the TVS as images and used the HT method described above to obtain parameters ***a*** (β) and ***b*** (K'), which describe the exponential shape of the spectrogram.

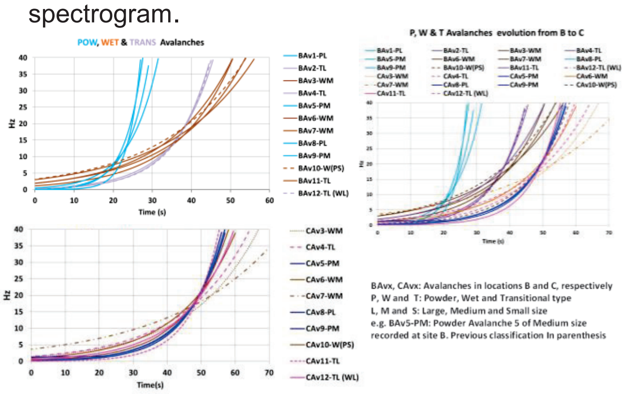

Figure 5. Curves corresponding to the different avalanches recorded at B (a) and C (b) and evolution from B to C (c). The avalanche types are represented by colors.

4. RESULTS

Table 1 displays the values K' and β and the standard deviations (σ) of the signals of the avalanches recorded at sites B and C. The standard deviation of K' is higher (not shown) than that of slope (β). The values obtained fall into different ranges according to the avalanche type. Table 2 shows the mean values of the three types of avalanche for the two sites and the ratio between them(E).

Type	β_{mB} (s^{-1})	β_{mc} (s^{-1})	$E=\beta_{mc}/\beta_{mB}$
POW	0.180	0.072	0.40
TRANS	0.095	0.080	0.84
WET	0.057	0.036	0.62

Table 2: Mean values of the three types of avalanche for the two sites and the ratio between them (E).

For site B, located upslope, the value of β (β_{mB}) for powder avalanches is greater than that for transitional avalanches and this value is, in turn, higher than that for the wet avalanches. At site C, located 690 m down slope, the behavior of the β values (β_{mC}) differs. The ratios between the β values for the two sites for the same type of avalanche E = β_{mC}/β_{mB} (Table 2) provide us with an index of the avalanche evolution between the two sites. A value of E close to 1 indicates an absence of evolution. The largest value obtained is the E value for transitional avalanches whereas powder avalanches yield the lowest value, indicating a higher evolution. In order to visualize the different shapes of the SON sections and the avalanche evolution, the curves F (t) = K' $e^{\beta t}$ for the different K' and β (Table 1) are presented in Figures 5. The curves were shifted in time to compare their curvature. This shift does not affect the curvature and corrects the different origin of time of the spectrograms in the image processing. Note that the curves at site B are collapsed (are clustered) according to the avalanche type (Figure 5a and Table 1). The curves of the powder avalanches show a sharp increase in frequency which exceeds that of the transitional avalanches. Curves for wet avalanches present a gentler increase. The curves at site C (Figure 5b) are similar regardless of the avalanche type although the peculiarities of each type persist. Figure 5c shows the curves recorded at B and C for the three types of avalanche plotted together to show the evolution of the different types between the two sites. Note that the curves are gentler at C than at B. This plot helps us to interpret the values of E in Table 2.

4.1 Calculation of avalanche speeds

An estimate of the avalanche speeds can be made as follows $v_a = \frac{\beta}{\alpha(f)}$ (γ=0). The coefficient α (f) related to the intrinsic attenuation of the seismic waves is frequency dependent according to eq. (2). This value is not easy to determine. In the scientific community, there is an ongoing discussion on the selection of this value that depends on the ground characteristics. Some authors assume α as a constant and others consider it to be frequency dependent (Vilajosana et al., 2007; Saló et al., 2018). Note that if α is considered frequency dependent then so is the avalanche speed (which has a physical significance). In a preliminary stage we consider α frequency independent. In the absence of known α values, we use the avalanche speed values deduced from the GEODAR measurements (Köhler et al., 2016; 2018; McElwaine et al., 2017) to obtain an α value constant for the area. The value used is 0.0026 m^{-1} obtained from the data of AV4 (Table 1). The avalanche speeds obtained using the values of β (Table 1) and those from GEODAR data are shown in Figure 6 and in Table 3. Although, regrettably, the error bars are high, the values of the avalanche speed calculated from GEODAR data are, in general, close to the values calculated from the spectra. The values obtained indicate that powder avalanches are faster than transitional avalanches and these in turn are faster than wet ones, as expected.

Avalanche/ Type	V_B	error	VB_GD	Vc	error	Vc_GD
Av1 POW-L	70	258				
Av2 TRANS-L	42	182				
Av3 WET-M	27	42	30	4	11	
Av4 TRANS- L	38	25	38	4	3	4
Av5 POW- M	53	46	34	7	15	21
Av6 WET-M	17	7	21	5	2	
Av7 WET-M	21	36	23	3	1	
Av8 POW-L	118	38	40	7	6	38
Av9 POW-M	84	99		8	3	
Av10 WET-S	18	18		7	6	15
Av11 TRANS-L	23	13	31	10	74	9
Av12 TRANS-L	42	30	18	6	7	5

Table 3: Avalanche speeds (ms^{-1}) at B (V_B) and C (V_C) obtained using the values of β (Table 1) and those deduced from GEODAR data (V_{GD}) (Köhler et al., 2016;2018; McElwaine et al., 2017).

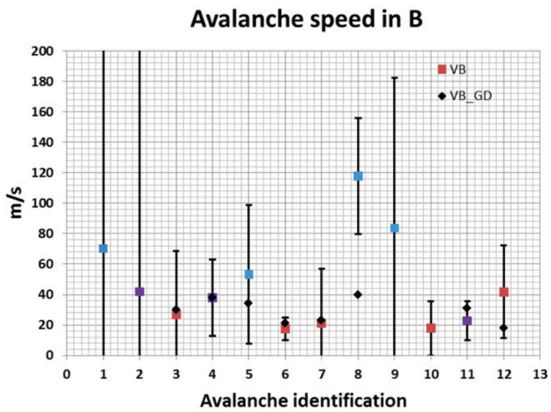

Figure 6: Representation of the avalanche speeds at B (VB) with error bars and those obtained from GEODAR (VB_GD) (Table 3). Colors: Blue POW; Black: WET; Lilac: TRANS.

5. CONCLUSIONS

The dependence of the shape of the SON section of a spectrogram of the signals generated by snow avalanches on the different contributors was obtained theoretically. This allowed us to obtain the parameters that reproduce the shape of the SON section of the spectrograms and to analyze their behavior. Spectrograms of the Total Seismic Signals of twelve avalanches recorded at two sites 690 m apart were calculated. When considering the spectrograms as images, we were able to quantify the shape of the SON sections using interactively the Hough Transform. The shapes are different for the three types of snow avalanches (POW, TRANS, and WET). An evolution of the shape of the spectrograms of the signals recorded at the two sites was observed. This evolution is different for the three avalanche types. Avalanche speed estimates were deduced from the parameters obtained. The computed avalanche speeds are consistent with the speed values derived directly from experimental field measurements for transitional and wet avalanches, although the speed values deduced for powder avalanches are in general overestimated.

ACKNOWLEDGMENTS

This study is supported by the MINECO Spanish projects CHARMA (ref. CGL2013-40828-R) and PROMONTEC (CGL2017-84720-R (AEI/FEDER, UE). We are indebted to the personnel of SLF (DAVOS), especially to B. Sovilla, for their help and support. E.S. received a grant from the Instituto de Geofísica, UNAM, México.

REFERENCES

Hough, P.V.C., 1962. Method and means for recognizing complex patterns. US Patent 3069654. Washington, DC, Patent and Trademark Office.

Köhler, A., J. N. McElwaine, B. Sovilla, M. Ash, and P. Brennan, 2016: The dynamics of surges in the 3 February 2015 avalanches in Vallée de la Sionne, J. Geophys. Res. Earth Surf., 121, 2192–2210, doi:10.1002/2016JF003887.

McElwaine*, J. N., A. Köhler*, B. Sovilla, M. Ash, and P. V. Brennan (2017), GEODAR data of snow avalanches at Vallée de la Sionne: Seasons 2010-2015[Data set], Zenodo, doi: 10.5281/zenodo.1042108, *eqlly contributing authors

Ridler, T.W. and S. Calvard, 1978. Picture thresholding using an iterative selection method. IEEE Transactions on Systems, Man and Cybernetics 8, 630-632.

Pérez-Guillén, C., B. Sovilla, E. Suriñach, M. Tapia and A. Köhler, 2016. Deducing avalanche size and flow regimes from seismic measurements. Cold Reg. Sci. Technol., 108,149-162. doi.org/10.1016/j.coldregions.2015.10.004.

Saló , L., J. Corominas , N. Lantada , G. Matas , A. Prades, and R. Ruiz-Carulla, 2018: Seismic Energy Analysis as Generated by Impact and Fragmentation of Single-Block Experimental Rockfalls. J. Geophys. Res. Earth Surf., 123. https://doi.org/10.1029/2017JF004374.

Sovilla, B., J. McElwaine, W. Steinkogler, M. Hiller, F. Dufour, E. Suriñach, C. Pérez-Guillén, J.-T. Fischer, E. Thibert, and D. Baroudi, 2013: The full-scale avalanche dynamics test site Vallée de la Sionne, in International Snow Science Workshop, Grenoble–Chamonix Mont-Blanc, France., pp.1350-1357.

Stein, S. and M. Wysession, 2003: An Introduction to Seismology, Earthquakes and Earth Structure. Blackwell Publishing.

Suriñach, E., G. Furdada, F. Sabot, B. Biescas, and J.M. Vilaplana, J.M., 2001: On the characterization of seismic signals generated by snow avalanches for monitoring purposes. Ann. Glac., 32: 268-274.

Vilajosana, I., E. Suriñach, G. Khazaradze, and P. Gauer, 2007: Snow avalanche energy estimation from seismic signal analysis. Cold Regions Science and Technology, 50, 72–85. doi:10.1016/j.coldregions.2007.03.007.